Inorganic Chemistry

Article

pubs.acs.org/IC

Preparation of a Homologous Series of Tetraalkylammonium Graphite Intercalation Compounds

Weekit Sirisaksoontorn and Michael M. Lerner*

Department of Chemistry, Oregon State University, Corvallis, Oregon 97331-4003, United States

ABSTRACT: Graphite intercalation compounds (GICs) of a series of symmetric or asymmetric tetraalkylammonium (TAA) intercalates are obtained from stage-1 $[Na(en)_{1.0}]C_{15}$ via cation exchange. The prepared dull-black TAA-GICs contain either flattened monolayer or bilayer galleries, with significant cointercalation of the dimethylsulfoxide (DMSO) solvent in the bilayer galleries. The TAA-GIC products obtained are characterized by X-ray diffraction and related structural modeling, compositional analyses, and Raman spectroscopy. $[(C_4H_9)_4N]C_{43}$ is obtained as a pure stage-1 GIC with the flattened monolayer structure. The larger symmetric TAA cations, $(C_6H_{13})_4N$, $(C_7H_{15})_4N$, $(C_8H_{17})_4N$, and the asymmetric TAA cations, $(C_{12}H_{25})(CH_3)_3N$, $(C_{18}H_{37})(CH_3)_3N$, $(C_{18}H_{37})_2(CH_3)_2N$, all form pure stage-1 GICs with flattened bilayer conformations. Thermogravimetric analyses combined with mass spectrometry and elemental analyses indicate the presence of ~1−2 DMSO cointercalates per bilayer cation. The intercalate layers in these TAA-GICs have expansions along the stacking direction of ~0.40 nm. Raman data confirm the low graphene sheet charge densities in the obtained TAA-GICs.

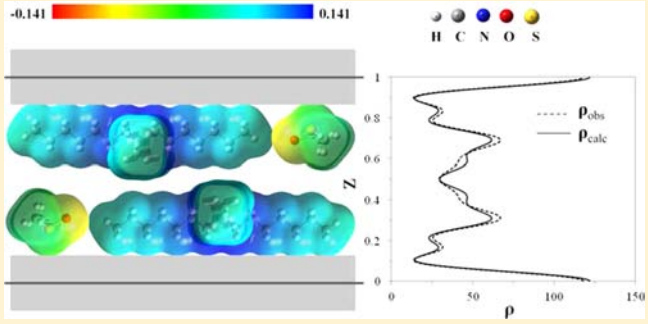

INTRODUCTION

Graphite has been long studied as an intercalation host and shows some unique aspects.[1−3] Graphite intercalation compounds (GICs) consist of host graphene layers and intercalate guests; either donor or acceptor-type compounds can be prepared by reduction or oxidation of the graphene sheets, respectively.[4−11] This redox intercalation can be performed by either chemical or electrochemical methods, and a wide range of atomic or molecular ions, often accompanied by neutral cointercalate molecules, are known to act as intercalate guests.[12−17] The ordered sequencing of intercalate and graphene sheets perpendicular to the stacking direction is known as "staging" in common for GICs,[18,19] and, while known, it is rarely observed with other layered hosts.[20] The highest intercalate contents are for stage-1 GICs, where all graphene sheets are separated by intercalate layers. Important applications for GICs and the associated chemistries include reversible energy storage in Li-ion battery anodes,[21,22] use as reducing agents[23] or gas/liquid absorbers,[24−26] and as precursors to exfoliated graphite or graphene.[27−31]

Our group has previously reported new donor-type GICs containing a wide range of alkali metal−amine intercalate complexes.[32−35] These GICs were prepared using a direct chemical approach where alkali metals and amines are simply combined with graphite under appropriate conditions. The arrangements and orientations of intercalates in the resulting GICs depend on both the alkali metal cation and the amine. For example, in $[Na(n\text{-}C_3H_7NH_2)_{0.7}]C_{16}$, the intercalate complexes are arranged as a monolayers with long molecular axes parallel to the encasing graphene layers.[32] Amine intercalates with longer alkyl substituents, such as in $[Na(s\text{-}C_4H_9NH_2)_{1.6}]C_{18}$, form intercalate bilayers, again with long molecular axes parallel to the graphene sheets.[32] Earlier studies on alkylammonium intercalation in graphite have employed electrochemical reduction in aprotic polar solvents.[16,36−41] Recently, our group reported a new chemical method for the preparation of a GIC containing tetrabutylammonium cations, by reaction in *N*,*N*-dimethylformamide (DMF), to displace the $Na(en)^+$ intercalate in $[Na(en)_{1.0}]C_{15}$ (en = ethylenediamine).[42] In that study, a stage-1 $[(C_4H_9)_4N]C_{44}$ GIC was obtained with a highly flattened intercalate monolayer and gallery expansion of 0.47 nm. We proposed that this cation conformation results from the large lattice enthalpies in GICs that strongly favor minimal expansion upon intercalation. No other tetraalkylammonium (TAA) GICs could be obtained using this approach.

The intercalation of alkylammonium ions via ion exchange has been widely studied for several layered hosts, along with detailed structural characterization of the resulting materials.[43−47] Highly flattened conformations have been observed previously.[48−51] For example, in smectite clays, a structural evolution from monolayer to bilayer to pseudotrilayer galleries is observed for increasing size of symmetric alkylammonium cations.[52,53] The intercalate monolayers showed an interlayer expansion of ~0.5 nm relative to the anhydrous host, requiring that the alkyl chain substituents lie parallel to the clay layers and that the cations have a flattened conformation. The interlayer spacing increases by an additional 0.4−0.5 nm for each added cation layer. Flattened monolayers of ~0.5 nm thickness were

Received: March 25, 2013
Published: May 31, 2013

   dx.doi.org/10.1021/ic400733k | *Inorg. Chem.* 2013, 52, 7139−7144

also observed in MoS_2, rectorite, and montmorillonite compounds with asymmetric alkylammonium intercalates.[54−56] These very small interlayer dimensions are at the steric limit of an alkylammonium headgroup.

In the present work, we report the first preparation of a homologous series of symmetric or asymmetric tetra-*n*-alkylammonium GICs (TAA-GICs) by adapting the previously reported method, and characterize structures and compositions of the GICs obtained.

EXPERIMENTAL PROCEDURE

Materials. Graphite powder (SP-1 grade, average diameter 100 μm) was used as received from Union Carbide, Inc. Ethylenediamine (99%), dimethylsulfoxide (AR grade, 99.9%), acetonitrile (HPLC grade, 99.9%), and anhydrous methanol (99.9%) were dried over a 4 Å molecular sieve prior to use. All tetraalkylammonium cations were obtained as bromide salts with a purity >98% and were used as received.

Syntheses. $[Na(en)_{1.0}]C_{15}$ (en = ethylenediamine) was prepared according to a previously reported reaction:[33] 20 mmol of graphite (240 mg) and 2 mmol of sodium metal (50 mg) were added to 3 mL of ethylenediamine and continuously stirred at 60 °C for 24 h under an inert atmosphere. After the supernatant solution was separated by centrifugation, a blue solid product was dried in vacuo overnight at room temperature. The product was characterized by PXRD and TGA, and used as a reagent for subsequent reactions.

For the ion exchange reactions with smaller TAA cations (e.g., $(CH_3)_4N$, $(C_2H_5)_4N$, $(C_3H_7)_4N$, $(C_4H_9)_4N$, and $(C_{12}H_{25})(CH_3)_3N$), 2 mL of dimethylsulfoxide (DMSO) was added to a reaction tube containing 0.30 mmol of $[Na(en)_{1.0}]C_{15}$ and 0.20 mmol of the alkylammonium bromide salt. The exchange was carried out at 60 °C for 10 min under an inert atmosphere. Next, the mixture was centrifuged for 5 min, and the top liquid phase was removed by syringe. The wet product was washed with acetonitrile and then anhydrous methanol to remove soluble byproducts and excess alkylammonium salt. The GIC product was dried in vacuo overnight at ambient temperature. The reactant solution and rinse solvents were collected, combined, and later analyzed to quantify the extent of the exchange.

The same synthetic procedure was employed for the larger TAA cations (e.g., $(C_5H_{11})_4N$, $(C_6H_{13})_4N$, $(C_7H_{15})_4N$, $(C_8H_{17})_4N$, $(C_{18}H_{37})(CH_3)_3N$, and $(C_{18}H_{37})_2(CH_3)_2N$), except that the products were rinsed only with anhydrous methanol, and were dried at 60 °C for 6 h.

Characterization. Powder X-ray diffraction (PXRD) patterns were recorded using a Rigaku Miniflex II diffractometer with Ni-filtered Cu K_α radiation (λ = 0.15406 nm). All measurements were collected in the 2θ range from 3° to 60° at a scan speed of 5°/min. The relationship of the gallery height (d_i), repeat distance along *c*-axis (I_c), and stage number (n) is given by:

$$I_c = d_i - 0.335(n - 1) \quad (1)$$

where 0.335 nm corresponds to the thickness of a single graphene sheet. The interlayer expansion (Δd) refers to the difference between the gallery height of the GIC and the thickness of a single graphene sheet (i.e., $\Delta d = d_i - 0.335$ nm).

A Shimadzu TGA-50 thermogravimetric analyzer (TGA) was used to study the thermal behavior of GICs under flowing Ar/O_2 (20 mL/min) at a heating rate of 10 °C/min from ambient to 800 °C. A TA Q-600 TGA equipped with a Hiden HPR-20 QIC mass spectrometer was employed to track the evolution of DMSO at m/z = 63 in flowing N_2 at the same heating rate. CHN and S elemental analyses were performed by Micro-Analysis, Inc. (Wilmington, DE). A Witech confocal Raman microscope was used to collect Raman spectra (resolution = 4 cm^{-1}) with a 514 nm laser source. Capillary zone electrophoresis (CZE) analyses were performed on a HP ^{3D}CE instrument according to a previously described method.[42]

Energy-minimized structural models and mapped electron density surfaces for the "flattened" and "undistorted" conformations of the selected $(C_7H_{15})_4N$ cation and DMSO molecule were calculated using the hybrid density functional method (B3LYP) with a 6-31G basis set and the Gaussian 09W software.

One-dimensional electron density maps were generated from a centrosymmetric stage-1 cell in comparison between the observed PXRD data sets and the calculated structure models. The methodology has been described in detail previously.[11]

RESULTS AND DISCUSSION

For larger TAA cations, the generation of a series of single-phase, stage-1 TAA-GICs can be accomplished via cation exchange as illustrated in Scheme 1, where the $Na(en)^+$ cationic

Scheme 1. Synthetic Route to TAA-GICs

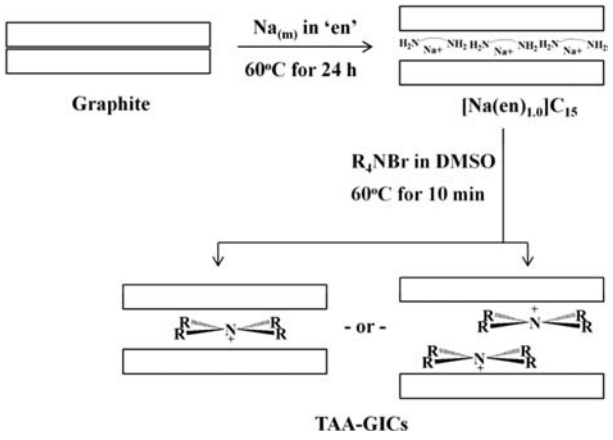

complex is displaced by TAA cations. For most of these reactions, the cation exchange occurs rapidly at moderate temperatures in a DMSO solvent. The color of all of the obtained GICs is dull black, as compared to the bright blue $[Na(en)_{1.0}]C_{15}$ reactant.

The PXRD patterns obtained for the reactant $[Na(en)_{1.0}]C_{15}$ and the TAA-GIC products are shown in Figure 1. $[Na(en)_{1.0}]C_{15}$ (Figure 1a) displays a highly ordered stacking arrangement with d_i = 0.691 nm. As reported previously, this gallery expansion is consistent with a monolayer arrangement of $Na(en)^+$ in which ethylenediamine forms a chelate structure oriented parallel to the graphene sheets.[33] Figure 1e shows the stage-1 $[(C_4H_9)_4N]C_{43}$ product obtained, with d_i = 0.813 nm. This product is similar to that obtained previously using exchange in DMF, and the interlayer expansion (Δd) of only 0.478 nm sterically requires the $(C_4H_9)_4N^+$ intercalates to form monolayers with a highly flattened conformation.[42]

Figure 1g−i shows the formation of several new, well-ordered, single-phase TAA-GICs. In each case, the observed reflections can be indexed as stage-1 GICs with $d_i \approx 1.14$ nm. No residual $[Na(en)_{1.0}]C_{15}$ is seen, although a very small graphite (002) reflection at $2\theta \approx 27°$ is often present, most notably in Figure 1g. The larger interlayer expansion ($\Delta d \approx 0.80$ nm), coupled with structure modeling and compositional data (described below), indicate that these large TAA intercalates form novel bilayer, rather than monolayer, galleries, again with the steric requirement that each layer contains highly flattened cations.

Exchange with $(C_5H_{11})_4N^+$ (Figure 1f) does not result in either the ordered monolayer or the bilayer arrangement, but yields instead a poorly ordered structure with only two strong

dx.doi.org/10.1021/ic400733k | Inorg. Chem. 2013, 52, 7139−7144

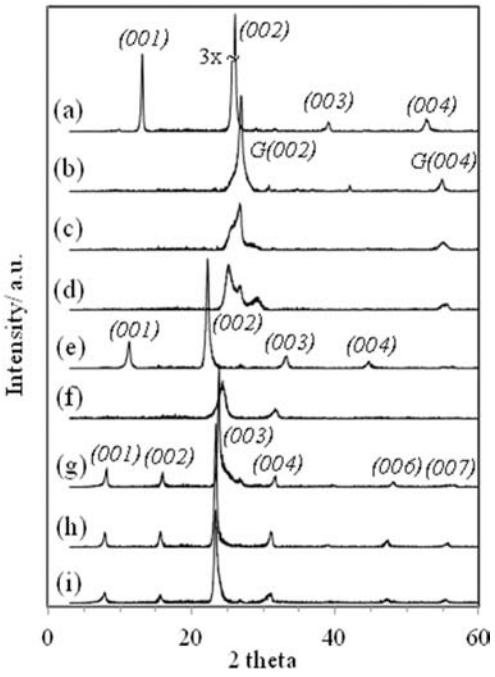

Figure 1. PXRD patterns of the (a) $[Na(en)_{1.0}]C_{15}$ reactant and GIC products containing (b) $(CH_3)_4N$, (c) $(C_2H_5)_4N$, (d) $(C_3H_7)_4N$, (e) $(C_4H_9)_4N$, (f) $(C_5H_{11})_4N$, (g) $(C_6H_{13})_4N$, (h) $(C_7H_{15})_4N$, and (i) $(C_8H_{17})_4N$. The assigned indices of obtained GICs and of graphite are denoted as (00*l*) and G(00*l*), respectively.

reflections observed. These are consistent with a stage-2 TAA-GIC with a bilayer gallery (Δd = 0.79 nm). Compositional analyses also show a lower intercalate content for this product (Table 1). The high angle shoulder on the (003) reflection after exchange with $(C_6H_{13})_4N^+$ (Figure 1g) may also be ascribed to a minor component of the stage-2 GIC.

Interestingly, attempts to exchange $[Na(en)_{1.0}]C_{15}$ with smaller TAA cations by the same route were unsuccessful; the products obtained after reaction with $(CH_3)_4N^+$ and $(C_2H_5)_4N^+$ cation-containing solutions show only broadened graphite reflections (Figure 1b,c), and the $(C_3H_7)_4N^+$ exchange reaction (Figure 1d) results in a mix of disordered graphite and a high-stage GIC. In these reactions, therefore, the oxidation of $[Na(en)_{1.0}]C_{15}$ to graphite or to a high-stage GIC must be accompanied by reduction of the reactant solution. Because $[Na(en)_{1.0}]C_{15}$ is oxidized to graphite by exposure to neat DMSO under similar conditions, we can restate these observations as the stabilization effect of the larger, but not the smaller, TAA cations that promotes ion exchange over GIC oxidation.

Although the products obtained after reaction with the larger TAA cations are stage-1GICs, the charge densities do decrease on the graphene sheets during these reactions, as will be shown below in the increased x value in the composition $[TAA]C_x$. This indicates a partial oxidation of the graphene sheets during the exchange process.

Figure 2a–c shows the PXRD patterns obtained following exchange with asymmetric TAA cations. All of the products

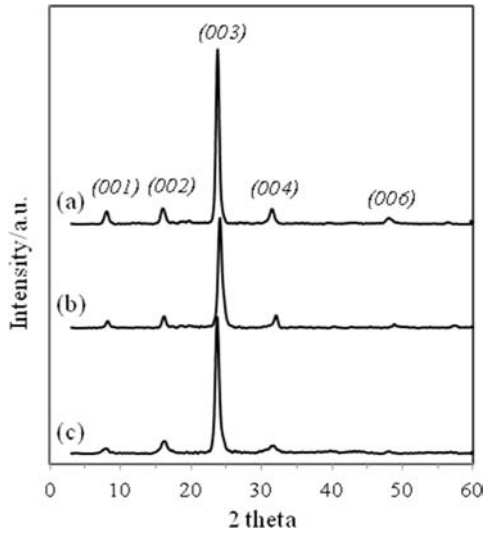

Figure 2. PXRD patterns of products obtained after exchange by asymmetric TAA cations (a) $(C_{12}H_{25})(CH_3)_3N$, (b) $(C_{18}H_{37})(CH_3)_3N$, and (c) $(C_{18}H_{37})_2(CH_3)_2N$.

obtained are single-phase, stage-1 GICs with $d_i \approx 1.12$ nm, indicating again a bilayer arrangement of flattened TAA cations. The structural data obtained for $[Na(en)_{1.0}]C_{15}$ and the TAA-GICs are summarized in Table 1.

Capillary zone electrophoretic (CZE) analyses can be used to quantitate soluble species during and after reactions, and here were used to monitor reaction progress and to determine GIC composition by the appearance of Na^+ and en and the disappearance of TAA cations from the reactant solution according to:

Table 1. Structural and Compositional Data of $[Na(en)1.0]C_{15}$ and Obtained TAA-GICs

cation	stage	d_i (nm)	Δd (nm)	intercalate arrangement	total intercalate (mass %)	composition	packing fraction
$Na(en)_{1.0}$[a]	1	0.691	0.356	monolayer	30.4	$[Na(en)_{1.0}]C_{15}$	0.51
$(C_3H_7)_4N$	high-stage + graphite	0.760	0.425	monolayer	11.8	n/a	n/a
$(C_4H_9)_4N$	1	0.813	0.478	monolayer	31.8	$[(C_4H_9)_4N]C_{43}$	0.55
$(C_5H_{11})_4N$	2	1.123	0.793	bilayer	27.5	n/a	n/a
$(C_6H_{13})_4N$	1	1.122	0.787	bilayer	38.2	$[(C_6H_{13})_4N]C_{59}$·1.1DMSO	0.42
$(C_7H_{15})_4N$	1	1.144	0.809	bilayer	40.8	$[(C_7H_{15})_4N]C_{63}$·1.4DMSO	0.45
$(C_8H_{17})_4N$	1	1.148	0.813	bilayer	41.4	$[(C_8H_{17})_4N]C_{76}$·1.9DMSO	0.46
$(C_{12}H_{25})(CH_3)_3N$	1	1.109	0.774	bilayer	38.8	$[(C_{12}H_{25})(CH_3)_3N]C_{44}$·1.4DMSO	0.43
$(C_{18}H_{37})(CH_3)_3N$	1	1.126	0.791	bilayer	37.5	$[(C_{18}H_{37})(CH_3)_3N]C_{60}$·1.6DMSO	0.40
$(C_{18}H_{37})_2(CH_3)_2N$	1	1.118	0.783	bilayer	41.4	$[(C_{18}H_{37})_2(CH_3)_2N]C_{85}$·2.2DMSO	0.48

[a]Data from ref 33.

dx.doi.org/10.1021/ic400733k | Inorg. Chem. 2013, 52, 7139–7144

$$[\mathrm{Na(en)}_{1.0}]\mathrm{C}_{15} \xrightarrow{\text{excess TAA+}} [\mathrm{TAA}]\mathrm{C}_x + a\mathrm{Na}^+ + b(\mathrm{en}) \quad (2)$$

where a, b, and x in the products can be derived directly from CZE data. Quantitative displacement of the sodium complex will result in $a = b = 1.0$. For exchanges using symmetric TAA cations larger than $(C_3H_7)_4N^+$, and for the asymmetric TAA cations, the exchange is nearly complete for both Na cations and en (the a and b values obtained are close to 1 in Table 2). Additionally, the TAA cation contents for the GICs derived from CZE(x) are consistent with TGA results (Table 2).

Table 2. Stoichiometric Ratios for Displacement Reaction 2 As Determined by CZE[a]

	CZE			TGA
obtained GICs	a	b	x	x
$[(C_4H_9)_4N]C_x$	0.97	1.0	41	43
$[(C_6H_{13})_4N]C_x$	1.0	0.98	56	59
$[(C_7H_{15})_4N]C_x$	1.0	1.0	58	63
$[(C_8H_{17})_4N]C_x$	1.0	0.99	63	72
$[(C_{12}H_{25})(CH_3)_3N]C_x$	0.97	0.93	40	44

[a] $[TAA]C_x$ values derived from TGA are also provided.

The thermal behavior of two TAA-GICs and graphite is shown in Figure 3. $[(C_4H_9)_4N]C_{43}$ shows two mass loss regions

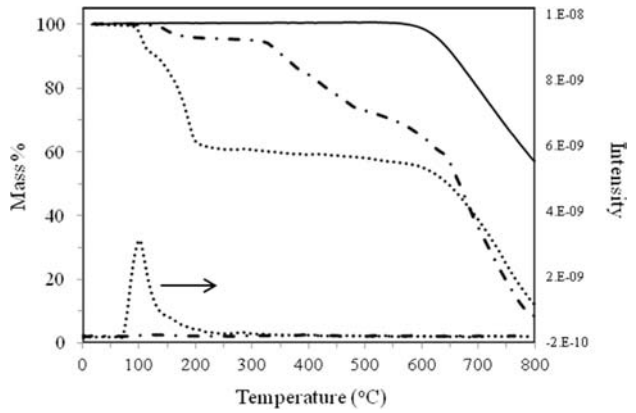

Figure 3. TGA mass loss data for $[(C_7H_{15})_4N]C_{63}$·1.4DMSO (···), $[(C_4H_9)_4N]C_{43}$ (– · – · –), and unreacted graphite (–). At the bottom, m/z = 63 peak intensities from TGA/MS are shown for $[(C_7H_{15})_4N]C_{63}$·1.4DMSO (···) and $[(C_4H_9)_4N]C_{43}$ (– · – · –).

(130–250, 250–500 °C) attributed to the thermolysis of the TAA cation. $[(C_7H_{15})_4N]C_{63}$·1.4DMSO shows a much larger total mass loss, and an additional low-temperature mass loss at 95–110 °C. The latter is ascribed to volatilization of a DMSO cointercalate, and this is confirmed by both the corresponding DMSO mass peak at m/z = 63 in the same temperature range and the subsequent elemental analysis for sulfur (3.5% S vs 3.4% S_{calc} from the actual composition in Table 1). Significant DMSO cointercalation was observed for all of the bilayer GICs, but neither the DMSO mass loss peak, nor any appreciable sulfur content, were identified in the monolayer gallery structure of $[(C_4H_9)_4N]C_{43}$. Mass loss above 550 °C for all samples including graphite is due to the combustion of a graphitic carbon by O_2 in the flow gas. On the basis of the CZE, TGA, and sulfur content analyses, the structural compositions of all resulting TAA-GICs are reported in Table 1 for the single-phase, or nearly single-phase, products. The exchanged products with $(C_3H_7)_4N^+$ and $(C_5H_{11})_4N^+$ are not included as they are multiphase. Again, it is interesting to note that only the TAA-GICs with bilayers incorporate DMSO into the intercalate galleries.

The packing fractions of these intercalate galleries can be calculated from the structural and compositional data reported above, and then compared to those in other GICs. Packing fraction is defined here as:

$$\text{packing fraction} = \frac{V_i}{V_h} \quad (3)$$

where V_i is the van der Waals volume of intercalates per formula unit, which is estimated by the VABC (atomic and bond contributions of van der Waals volume) method,[57] and V_h is the available volume per formula unit due to the lattice expansion obtained from the surface area per graphitic carbon (0.0261 nm^3), product composition, and the observed Δd. The resulting packing fractions are provided in Table 1, and show a range of 0.40–0.55, with the monolayer gallery in $[(C_4H_9)_4N]C_{43}$ showing more dense intercalate packing than any of the bilayer arrangements.

To model the bilayer arrangement of flattened intercalates and DMSO cointercalates, a 1-D electron density map along the c-axis direction was generated from the PXRD (00l) peak intensities. The calculated profile for a structure model of $[(C_7H_{15})_4N]C_x$·1.4DMSO is compared to that obtained from observed PXRD peak intensities (Figure 4). In the model, the

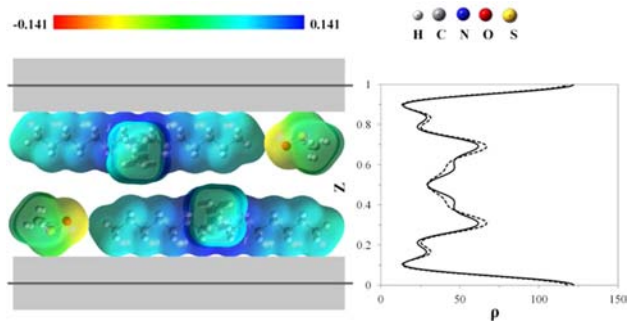

Figure 4. Structure model and 1D-electron density profiles for $[(C_7H_{15})_4N]C_x$·1.4DMSO showing the bilayer intercalate arrangement. The dashed line and solid line represent the profiles derived from observed data and from the structure model, respectively (the crystallographic R factor = 0.11).

flattened TAA conformations are generated using Gaussian, and bilayers are formed with these cations oriented with long axes parallel to the graphene sheets. The DMSO cointercalates are positioned with H and S atoms nestled into the graphene sheets by 0.038 and 0.032 nm, respectively. The relative concentrations of TAA and DMSO within galleries were fixed by the known product compositions. The close agreement of model and observed profiles obtained can be seen in Figure 4. Multiple models were tested, and we conclude that the double peak of electron density from the observed data is only consistent with a bilayer intercalate model. However, the best fit model indicates an x value considerably lower than that observed (37 vs 63). The origin of this mismatch is under investigation.

The Raman spectrum of pristine graphite (Figure 5a) exhibits a strong G-band at 1584 cm^{-1} (E_{2g}) involving

dx.doi.org/10.1021/ic400733k | Inorg. Chem. 2013, 52, 7139–7144

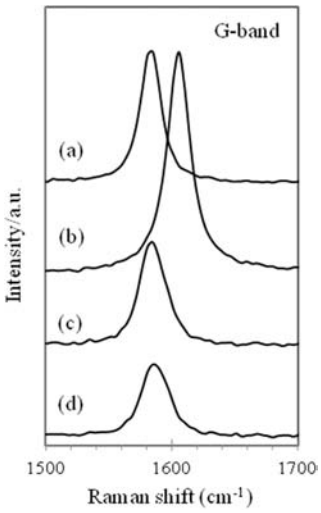

Figure 5. Raman spectra for (a) pristine graphite, (b) $[Na(en)_{1.0}]C_{15}$, (c) $[(C_4H_9)_4N]C_{43}$, and (d) $[(C_7H_{15})_4N]C_{63}$·1.4DMSO.

intralayer atomic motion. Reductive intercalation into the graphitic host causes a perturbation of the in-plane force constant, resulting in a G-band shift to higher frequency. The magnitude of the shift has been shown to depend on the degree of reduction, and therefore the stage, of the GIC formed.[58−60] $[Na(en)_{1.0}]C_{15}$ (Figure 5b) shows a significant shift to a peak maximum at 1605 cm^{-1}. The G-band peak positions for $[(C_4H_9)_4N]C_{43}$ and $[(C_7H_{15})_4N]C_{63}$·1.4DMSO (Figure 5c,d) are both at 1586 cm^{-1}. These peak positions agree with the conclusion drawn from the compositional data, that these GICs have very low charge densities for stage 1 GICs.

To our knowledge, the observed range of x from 41 to 85 in these TAA-GICs indicates the lowest charge densities for any stage-1 reduced GICs.[1] The very low charge densities are required by the steric demands (i.e., large footprints) of the monovalent, flattened TAA cations. Thus, designed intercalation of large deformable cations provides a degree of steric control over the sheet charge densities in GICs. Sterics may also help explain the observed monolayer to bilayer transition, as the high packing fractions for $[(C_4H_9)_4N]C_{43}$ would necessarily increase even further if larger TAA cations adopted a monolayer arrangement. In future, the intercalation of even larger cations may generate tri- or multilayer galleries, or perhaps produce stable materials containing fully disordered (delaminated) graphene sheets.

CONCLUSION

A new series of stage-1 donor-type GICs containing TAA intercalates was successfully prepared via cation exchange in DMSO. Monolayer or bilayer arrangements of flattened intercalates are formed, with solvent cointercalation observed only for the bilayer structures. TAA cations smaller than $(C_4H_9)_4N^+$ do not form stable GICs by this approach. These large intercalates diminish the charge densities on the graphene sheets in the GICs obtained.

AUTHOR INFORMATION

Corresponding Author

*E-mail: michael.lerner@oregonstate.edu.

Notes

The authors declare no competing financial interest.

ACKNOWLEDGMENTS

We thank Professor Vincent Remcho and Adeniyi Adenuga (OSU Chemistry) for assistance with CZE, and Professor Chih-Hung Chang and Changqing Pan (OSU Chemical Engineering) for assistance with Raman measurements.

REFERENCES

(1) Enoki, T.; Suzuki, M.; Endo, M. *Graphite Intercalation Compounds and Applications*; Oxford University Press: New York, 2003.
(2) Dresselhaus, M. S.; Dresselhaus, G. *Adv. Phys.* **2002**, *51*, 1.
(3) Chung, D. D. L. *J. Mater. Sci.* **2002**, *37*, 1475.
(4) Parry, G. S.; Nixon, D. E.; Lester, K. M.; Levene, B. C. *J. Phys. C* **1969**, *2*, 2156.
(5) Parry, G. S.; Nixon, D. E. *Nature* **1967**, *216*, 5118.
(6) Jones, J. E.; Cheshire, M. C.; Casadonte, D. J.; Phifer, C. C. *Org. Lett.* **2004**, *6*, 1915.
(7) Goutfer-Wurmser, F.; Herold, C.; Lagrange, P. *Carbon* **1996**, *34*, 821.
(8) Akuzawa, N.; Ikeda, M.; Amemiya, T.; Takahashi, Y. *Synth. Met.* **1983**, *7*, 65.
(9) Inagaki, M.; Ohira, M. *Carbon* **1993**, *31*, 777.
(10) Sorokina, N. E.; Maksimova, N. V.; Avdeev, V. V. *Inorg. Mater.* **2002**, *38*, 564.
(11) Zhang, X.; Lerner, M. M. *Chem. Mater.* **1999**, *11*, 1100.
(12) Mizutani, Y.; Abe, T.; Ikeda, K.; Ihara, E.; Asano, M.; Harada, T.; Inaba, M.; Ogumi, Z. *Carbon* **1997**, *35*, 61.
(13) Takenaka, A.; Tsumura, T.; Toyoda, M. *Synth. Met.* **2010**, *160*, 1247.
(14) Özmen-Monkul, B.; Lerner, M. M.; Pawelke, G.; Willner, H. *Carbon* **2009**, *47*, 1592.
(15) Moissette, A.; Fuzellier, H.; Burneau, A.; Dubessy, J.; Lelaurain, M. *Carbon* **1995**, *33*, 123.
(16) Bensenhard, J. O.; Möhwald, H.; Nickl, J. J. *Carbon* **1980**, *18*, 399.
(17) Okuyama, N.; Takahashi, T.; Kanayama, S.; Yasunaga, H. *Physica B/C* **1981**, *105*, 298.
(18) Thomas, J. M.; Millward, G. R.; Schlögl, R. F.; Boehm, H. P. *Mater. Res. Bull.* **1980**, *15*, 671.
(19) Sethuraman, V. A.; Hardwick, L. J.; Srinivasan, V.; Kostecki, R. *J. Power Sources* **2010**, *195*, 3655.
(20) Solin, S. A. *Annu. Rev. Mater. Sci.* **1997**, *27*, 89.
(21) Santhanam, R.; Noel, M. *J. Power Sources* **1998**, *72*, 53.
(22) Ogumi, Z.; Inaba, M. *Bull. Chem. Soc. Jpn.* **1998**, *71*, 521.
(23) Rashkov, I. B.; Panayotov, I. M.; Shishkova, V. C. *Carbon* **1979**, *17*, 103.
(24) Takahashi, Y.; Akuzawa, N.; Béguin, F. *Synth. Met.* **1995**, *73*, 45.
(25) Skowronski, J. M.; Krawczyk, P. *Solid State Ionics* **2010**, *181*, 653.
(26) Toyoda, M.; Inagaki, M. *Carbon* **2000**, *38*, 199.
(27) Kwon, O.-Y.; Choi, S.-W.; Park, K.-W.; Kwon, Y.-B. *J. Ind. Eng. Chem.* **2003**, *9*, 743.
(28) Inagaki, M.; Tashiro, R.; Washino, Y.; Toyoda, M. *J. Phys. Chem. Solids* **2004**, *65*, 133.
(29) Viculis, L. M.; Mack, J. J.; Kaner, R. B. *Science* **2003**, *299*, 1361.
(30) Makotchenko, V. G.; Grayfer, E. D.; Nazarov, A. S.; Kim, S.-J.; Fedorov, V. E. *Carbon* **2011**, *49*, 3233.
(31) Geng, Y.; Zheng, Q.; Kim, J.-K. *J. Nanosci. Nanotechnol.* **2011**, *11*, 1084.
(32) Maluangnont, T.; Sirisaksoontorn, W.; Lerner, M. M. *Carbon* **2012**, *50*, 597.
(33) Maluangnont, T.; Lerner, M. M.; Gotoh, K. *Inorg. Chem.* **2011**, *50*, 11676.
(34) Maluangnont, T.; Bui, G. T.; Huntington, B. A.; Lerner, M. M. *Chem. Mater.* **2011**, *23*, 1091.
(35) Maluangnont, T.; Gotoh, K.; Fujiwara, K.; Lerner, M. M. *Carbon* **2011**, *49*, 1033.
(36) Santhanam, R.; Noel, M. *J. Power Sources* **1995**, *56*, 101.
(37) Simonet, J.; Lund, H. *J. Electroanal. Chem.* **1977**, *75*, 719.

(38) Simonet, J. *Electrochem. Commun.* **2013**, *30*, 17.
(39) Katayama, Y.; Yukumoto, M.; Miura, T. *Electrochem. Solid-State Lett.* **2003**, *6*, A96.
(40) Zheng, H.; Li, B.; Fu, Y.; Abe, T.; Ogumi, Z. *Electrochim. Acta* **2006**, *52*, 1556.
(41) Zheng, H.; Jiang, K.; Abe, T.; Ogumi, Z. *Carbon* **2006**, *44*, 203.
(42) Sirisaksoontorn, W.; Adenuga, A. A.; Remcho, V. T.; Lerner, M. M. *J. Am. Chem. Soc.* **2011**, *133*, 12436.
(43) Liu, Z.-H.; Ooi, K.; Kanoh, H.; Tang, W.-P.; Tomida, T. *Langmuir* **2000**, *16*, 4154.
(44) Kanzaki, Y.; Konuma, M.; Matsumoto, O. *J. Phys. Chem. Solids* **1980**, *41*, 525.
(45) Sasaki, T.; Watanabe, M. *Mol. Cryst. Liq. Cryst.* **1998**, *311*, 417.
(46) Letaief, S.; Detellier, C. *Clays Clay Miner.* **2009**, *57*, 638.
(47) Liu, Z.-H.; Wang, Z.-M.; Yang, X.; Ooi, K. *Langmuir* **2002**, *18*, 4926.
(48) Xi, Y.; Frost, R. L.; He, H.; Kloprogge, T.; Bostrom, T. *Langmuir* **2005**, *21*, 8675.
(49) Peng, S.; Gao, Q.; Du, Z.; Shi, J. *Appl. Clay Sci.* **2006**, *31*, 229.
(50) Nakayama, M.; Konishi, S.; Tagashira, H.; Ogura, K. *Langmuir* **2005**, *21*, 354.
(51) Jaynes, W. F.; Boyd, S. A. *Soil Sci. Soc. Am. J.* **1991**, *55*, 43.
(52) Mercier, L.; Detellier, C. *Clays Clay Miner.* **1994**, *42*, 71.
(53) Chun, Y.; Sheng, G.; Boyd, S. A. *Clays Clay Miner.* **2003**, *51*, 415.
(54) Li, Z.; Jiang, W. T. *Thermochim. Acta* **2009**, *483*, 58.
(55) Golub, A. S.; Zubavichus, Ya. V.; Slovokhotov, Yu. L.; Novikov, Yu. N.; Danot, M. *Solid State Ionics* **2000**, *128*, 151.
(56) He, H.; Frost, R. L.; Bostrom, T.; Yuan, P.; Duong, L.; Yang, D.; Xi, Y.; Kloprogge, J. T. *Appl. Clay Sci.* **2006**, *31*, 262.
(57) Zhao, Y. H.; Abraham, M. H.; Zissimos, A. M. *J. Org. Chem.* **2003**, *68*, 7368.
(58) Doll, G. L.; Eklund, P. C.; Fischer, J. E. *Phys. Rev. B* **1987**, *36*, 4940.
(59) Vora, P.; York, B. R.; Solin, S. A. *Synth. Met.* **1983**, *7*, 355.
(60) Dresselhaus, M. S.; Dresselhaus, G. *Top. Appl. Phys.* **1982**, *51*, 3.